Surface Normal Coupling to Multiple-Slot and Cover-Slotted Silicon Nanocrystalline Waveguides and Ring Resonators

John Covey, Ray T. Chen

Dept. Electrical and Computer Engineering, The University of Texas at Austin, 10100 Burnett Rd, PRC/MER 160, Austin, TX 78758, USA.
Author e-mail address: john.covey@coveytech.com, raychen@uts.cc.utexas.edu

Abstract

Grating couplers are ideal for coupling into the tightly confined propagation modes of semiconductor waveguides. In addition, nonlinear optics has benefited from the sub-diffraction limit confinement of horizontal slot waveguides. By combining these two advancements, slot-based nonlinear optics with mode areas less than 0.02 μm^2 can become as routine as twisting fiber connectors together. Surface normal fiber alignment to a chip is also highly desirable from time, cost, and manufacturing considerations. To meet these considerable design challenges, a custom genetic algorithm is created which, starting from purely random designs, creates a unique four stage grating coupler for two novel horizontal slot waveguide platforms. For horizontal multiple-slot waveguides filled with silicon nanocrystal, a theoretical fiber-to-waveguide coupling efficiency of 68% is obtained. For thin silicon waveguides clad with optically active silicon nanocrystal, known as cover-slot waveguides, a theoretical fiber-to-waveguide coupling efficiency of 47% is obtained, and 1 dB and 3 dB theoretical bandwidths of 70 nm and 150 nm are obtained, respectively. Both waveguide platforms are fabricated from scratch, and their respective on-chip grating couplers are experimentally measured from a standard single mode fiber array that is mounted surface normally. The horizontal multiple-slot grating coupler achieved an experimental 60% coupling efficiency, and the horizontal cover-slot grating coupler achieved an experimental 38.7% coupling efficiency, with an extrapolated 1 dB bandwidth of 66 nm. This report demonstrates the promise of genetic algorithm-based design by reducing to practice the first large bandwidth vertical grating coupler to a novel silicon nanocrystal horizontal cover-slot waveguide.

Keywords: optical interconnects, grating couplers, horizontal slot waveguides, nonlinear optics, silicon nanocrystal, cover slot waveguides, vertical coupling, genetic algorithms

1. INTRODUCTION

Slot waveguides are a powerful new platform for integrated optics due to their ability to confine a guided mode into areas smaller than the diffraction limit. However, due to the extreme confinement of light within the waveguide slots, scattering losses from such waveguides are extremely sensitive to thickness variations and/or roughness along an interface. Because of this sensitivity, horizontally confined slot waveguides, where the light is confined parallel to the substrate, are advantageous when compared to vertical slots, as deposition, oxidation, and/or epitaxial growth can all routinely achieve near atomic flatness even for films only a few nanometers thick. This results in improved propagation losses for amorphous and polycrystalline silicon (polysilicon) horizontal slot waveguides (3 & 7 dB/cm, respectively) [1, 2] when compared to vertical slot waveguides of single-crystal silicon (11.6 dB/cm) [3].

While crystalline/amorphous silicon slot waveguides have lower propagation losses than their polysilicon counterpart, having a robust polysilicon slot platform is still advantageous for three reasons. First, multiple slot configurations are obtainable with multiple deposited silicon layers, which can further confine light to narrower slot regions [4]. Second, the extra polysilicon layers can be doped and made electrically active in order to create tunable and switchable electro-optic devices [2]. Third, unlike hydrogen-passivated amorphous silicon layers, polysilicon withstands a very high thermal budget, allowing for far greater process flexibility. For example, silicon nanocrystal oxide is commonly utilized as a slot material for its high nonlinear optical coefficients when annealed at high temperatures [5, 6]. Thus, further

Optical Interconnects XIV, edited by Henning Schröder, Ray T. Chen, Alexei L. Glebov,
Proc. of SPIE Vol. 8991, 89911A · © 2014 SPIE · CCC code: 0277-786X/14/$18
doi: 10.1117/12.2044231

enabling a polysilicon, multi nanocrystal slotted platform for ongoing all-optical and electro-optical device characterization efforts is a necessity.

Despite these advantages for polysilicon, crystalline silicon may still remain the dominant substrate of choice due to its material purity. availability, low cost, and ubiquitous use for electronic semiconductor applications. Thus, designing, fabricating, and optically coupling to a simple, readily available platform which allows for horizontally slotted confinement in crystalline silicon is also highly desirable. In order to simplify fabrication as much as possible, cover-slotted crystalline silicon waveguides, where the slot confinement appears in the waveguide cladding, are investigated. Although nonlinear optical switching has been demonstrated in cover-slotted crystalline silicon waveguides, fiber-to-waveguide coupling to this particular propagation mode has not received adequate attention to date [7].

Despite silicon nanocrystals being lauded as a possible monolithic, on-chip laser source [8], sufficient lasing output has yet to be reported for any silicon medium, and consequently, external fiber-coupled light remains the dominant form of enlightening any silicon platform. Although inverse-tapered coupling structures have been proposed for horizontal slot waveguide fiber coupling [9], lensed fibers are required, and only small translation errors are acceptable. In comparison, grating couplers are becoming an increasingly preferred solution for both the silicon-on-insulator platform [10-14] as well as for horizontal slot waveguides [15, 16]. Properly designed gratings may couple to standard single mode fiber with high efficiency and fiber translation tolerance without any need for cleaving, dicing, or polishing, allowing for timely in-line wafer testing.

Nevertheless, two issues remain which potentially impede the mass-manufacturability of horizontal slot grating couplers. First, obtaining acceptable coupling efficiencies without adding precise grating overlay deposition and lithography steps [10] is desirable from a manufacturing perspective. Second, nearly all grating couplers demonstrated to date require angular detuning of the input/output fibers by a significant angle from normal incidence (~8-12 degrees) in order to eliminate significant back reflection and transmission problems [13]. High throughput testing and mounting of fibers and/or vertical-cavity-surface-emitting-lasers (VCSELs) that are perfectly normal to the substrate would drastically increase device packaging reliability while also reducing packaging complexity and cost. Furthermore, while grating couplers must emit at the proper azimuthal angle to couple to an angularly detuned fiber, this is not the case for normally incident, unpolarized fibers. Using non-tilted fibers significantly relaxes waveguide routing constraints near vertically emitting grating couplers.

Although surface normal grating couplers exhibit potential advantages over angularly detuned gratings, previous surface normal couplers on silicon waveguides have required extreme fabrication complexity [17], an extensive bottom reflector [18], extra high resolution fabrication steps [19], or significant expansion of the device's footprint by simultaneously coupling to two counter-propagating waveguides [20]. Such elaborate workarounds are due to grating couplers often being designed solely from first principles with a single period and fill factor, effectively eliminating two of the most significant degrees of freedom available to a designer. To circumvent the difficulty of relaxing first-principle design, previous works have employed a genetic algorithm to slightly vary a traditionally designed grating in order to obtain marginal efficiency increases [17, 19, 21]. However, entirely departing from an initial first-principle design could manifest new structures that enable high performance coupling across many platforms, specifications, and fabrication constraints.

In this work, input/output grating coupler pairs were created on two separate platforms: 1) partially-etched, dual horizontal nanocrystal slot waveguides and 2) nanocrystal horizontally cover-slotted waveguides. The designs were evolved via a genetic algorithm [22] (which is introduced in the following section) with no initial design, fabricated, and simultaneously coupled to and from a single mode fiber array at perfectly normal incidence.

2. DESIGN – GENETIC ALGORITHM

2.1 Multiple Horizontal Slot Waveguide Design

In order to efficiently and maximally explore the potential design space for a fiber-grating coupler, the etch depth, deposited film thickness, period, and fill factor of each individual grating tooth must be considered. While variable etch depth for each grating tooth is a possible approach in grating design [23], preliminary 2D FDTD results over all feasible

film thicknesses indicated that coupling efficiencies for slot waveguide gratings were not sensitive to etch depth as long as all slot layers were completely through-etched, as the slot layers contain the majority of guided light. In order to simplify fabrication without compromising coupling efficiency, all designs left the bottom silicon layer of the slot waveguide unetched, while all other waveguide layers were through-etched. This partially-etched profile yields higher emission toward the fiber and less emission toward the substrate through constructive and destructive vertical interference, respectively. Upward constructive interference was also maximized in 2D FDTD by fixing the buried oxide thickness to 2.38 μm. The number and thickness of waveguide layers were optimized in RSoft FemSIM to maximize slot field confinement in a single mode horizontal dual-slot waveguide, as shown in Fig. 1. After this optimization, the top and bottom polysilicon layers are 128 nm thick, the middle polysilicon layer is 33 nm thick, and the two silicon nanocrystalline oxide slots are 27 nm thick. Although field confinement and grating coupling efficiency were shown in simulations to be higher in three or four slot waveguides, two slots were ultimately chosen to reduce fabrication complexity and increase yield in our research-grade fabrication facility.

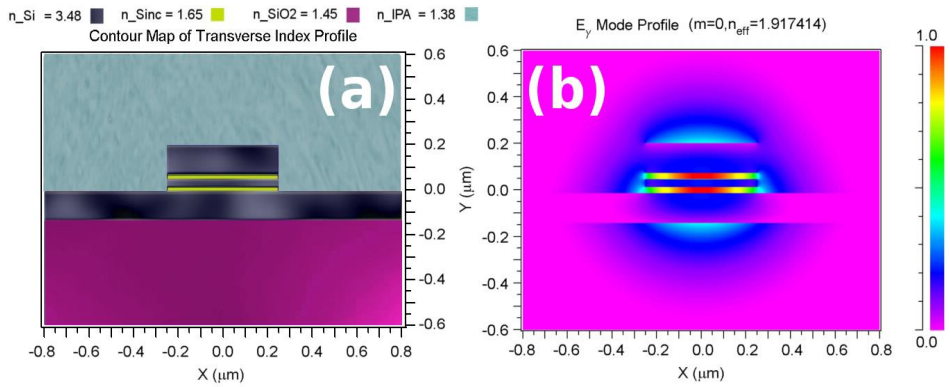

Fig. 1 (a) Rib-waveguide index profile obtained via partial etch. To simplify testing, isopropyl alcohol is the top cladding. The ripples in the polysilicon layers represent grain boundaries of approximate scale [24]. (b) TM mode profile of the multi-slot rib-waveguide, showing acceptable power confinement in the slots.

2.2 Horizontal Cover Slot Design

The cover-slotted waveguide design originates with our commercially available silicon-on-insulator wafers from SOITEC. The original silicon thickness is 250 nm, and the bottom oxide layer is 3 μm thick. Per the above section, this oxide layer is beyond the optimal thickness, which will be discussed in section 3.2. By oxidizing and HF etching the top silicon layer, any waveguide thickness below 250 nm is obtainable. To this end, RSoft FEMSIM was used to optimize the silicon thickness and waveguide width in order to maximize field intensity in the nonlinear silicon nanocrystalline oxide cladding. After optimization, the crystalline silicon waveguide is 120 nm thick, and the waveguide is 250 nm wide. In the original approach, only the silicon layer was etched and 300 nm of silicon nanocrystal was then blanket deposited. However, because the waveguides and gratings were etched together in a single step, preliminary FDTD grating simulations revealed insufficient index contrast for efficient grating emission, as most of the light propagates in the uninterrupted cladding, outside of the etched layer. Thus, the single etch step was altered to etch through both the nanocrystalline oxide cladding and the crystalline silicon, which approximately quadrupled the grating emission efficiency while having negligible impact on the guided mode profile. The resulting cover-slot mode, shown in Fig. 2, has 65% of the slot intensity of the multi-slot guide presented in section 2.1.

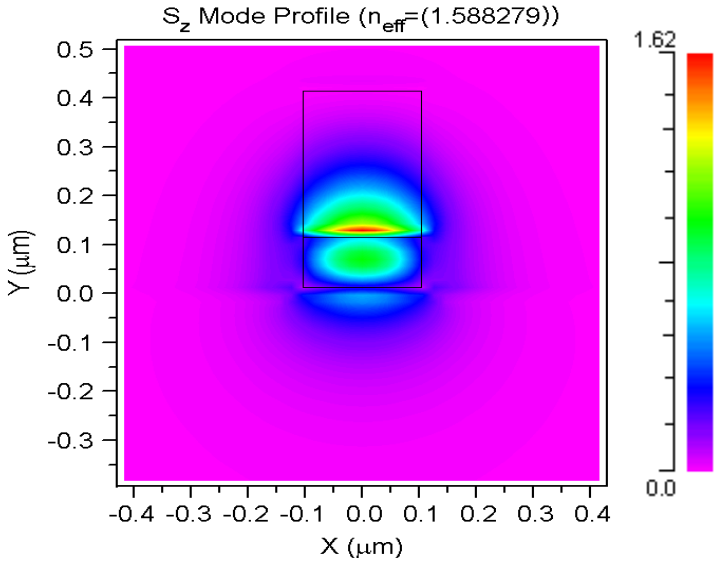

Fig. 2 TM mode profile of the cover-slot waveguide, showing high power confinement in the cladding directly above the silicon. The lower black rectangle outlines the crystalline silicon region, and the upper black rectangle outlines the silicon nanocrystalline cladding. The remaining upper cladding region is air, and the lower cladding is silicon oxide.

2.3 Genetic Algorithm

The two remaining design parameters for grating couplers are the period and fill factor. To maximally explore a grating's entire design space, individual grating teeth must be allowed different periods and fill factors. Because these parameters are no longer uniform for each grating tooth, the number of possible grating designs to consider increases geometrically. In order to find an optimum coupling efficiency despite this vast increase in design space, an in-house genetic algorithm was created from scratch where "genes" represent the period and fill factor of each grating tooth. Thus, the genetic code for a single grating design can consist of a number array of grating periods and fill factors. By programmatically converting this number array into a grating and inserting the structure into a photonic simulator capable of determining its fiber coupling efficiency, the "fitness" (coupling efficiency) of a particular "genetic code" (grating design) can be determined. After the efficiencies of many initial grating designs are obtained, the best designs within the group are selected to "mate" with each other in order to produce "children" grating designs. In the "mating" process, part of the number array of one grating design overwrites part of the number array of another grating design. In genetics, this process is known as "crossing over," and the resulting design retains characteristics from both parent designs. The newly created grating design then experiences "mutation," where a single number of its genetic code is randomly selected and randomly altered. This final step may also be considered a simulated-annealing or a Monte-Carlo-like step to sufficiently perturb designs to ensure the algorithm does not settle on local optima within the design space. After the new designs are created, the algorithm may repeat itself by evaluating the new designs and selecting those with the highest coupling efficiencies for subsequent iterations. Although the above approach can eventually reach the global optimum of a design space, a very large number of grating simulations are usually required to obtain it, as each genetic generation produces tens of new designs to evaluate, and thousands to tens of thousands of design generations may be necessary. A flow chart of the entire iterative genetic evolution process is shown in Fig. 3.

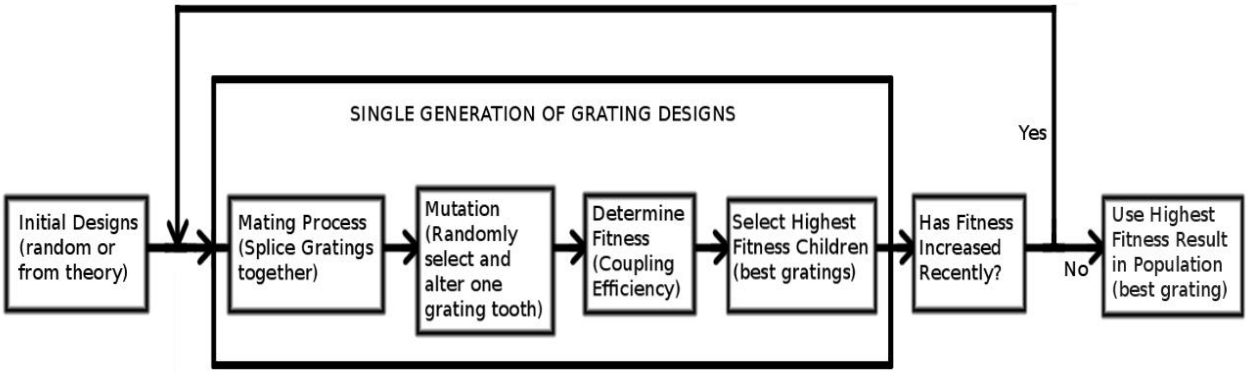

Fig. 3. Flow diagram of the iterative design process involved in evolving grating designs via a genetic algorithm.

For this particular design methodology to succeed over a realistic time interval, a single fiber-grating coupling efficiency must be simulated in tens of seconds or less. Because fiber-grating couplers usually contain strong index perturbations on scales near the wavelength of light, FDTD is most commonly used to simulate these structures. However, FDTD requires at least tens of minutes to complete a single grating simulation, which readily explains why grating couplers are typically designed solely from first principles, where uniform scattering and perfect phase-matching from an infinite number of periods are assumed in order to make the situation mathematically tractable. This limitation leaves designers with far fewer degrees of freedom than are physically possible. Fortunately, a fully vectorial eigenmode expansion and propagation tool, known as CAMFR, has been developed that is capable of simulating grating couplers with arbitrary cross-sections and strong index contrast in tens of seconds or less [25, 26]. By successfully integrating the custom-made genetic algorithm with CAMFR, the resulting grating design suite is capable of exploring a very large possibility space for a particular photonic platform in weeks to months instead of years to decades. A single, standard desktop operating at 4 GHz was able to complete all computational work for this report within two months.

3. SIMULATION

3.1 Multiple Slot Grating

Initially, a grating with 15 periods of 760 nm followed by 30 periods of 380 nm, all with 50% fill factor, was fed into the genetic algorithm as an initial starting design point, where the shorter period created a side reflecting distributed bragg reflector (DBR). Despite the design having a DBR to redirect non-emitted light and a buried oxide of proper thickness to reflect downward emitted light, the initial fiber coupling efficiency was 27%. After only 300 generations, the genetic algorithm plateaued at 40% efficiency. The design's initial period was then swept from 710 nm to 810 nm and fed into the genetic algorithm, all of which resulted in the same 40% efficient grating design. The only significant alteration accomplished by the genetic algorithm was to introduce apodization (where the fill factor is ramped) in order to more smoothly transition the incoming light into the grating's Bloch mode and reduce back reflections into the waveguide [12]. The algorithm also introduced slight randomization into the DBR section, the effect of which will be explored further in the final design.

This settling of various first-principle designs into the same local optima indicated that drastically different initial conditions were required to obtain a global optimum in the design space. To this end, designs with purely random periods and fill factors for each grating tooth were then fed into the genetic algorithm. After a few hundred generations, a large number of grating designs had already surpassed the 27% efficiency obtained by the original first-principle design. After 10,000 generations, the genetic algorithm plateaued with a 68% grating-to-fiber coupling efficiency. Although CAMFR only simulated the structure's waveguide-to-fiber coupling efficiency, 2D FDTD also yielded the same efficiency for fiber-to-waveguide coupling, as was expected via the reciprocity condition. The resulting structure and its emission profile are shown in Fig. 4.

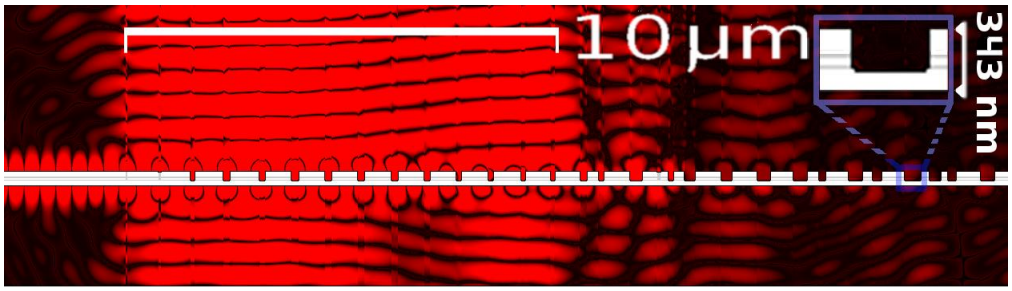

Fig. 4. Grating cross section showing simulated surface normal E-field emission to a fiber aperture from a waveguide on the left. Polysilicon is shown in white, and the silicon nanocrystalline oxide slots are in grey. The blue inset shows an enlarged view of a grating tooth. The etch depth for all sections is 215 nm.

In this final result, the genetic algorithm evolved a grating with four operational stages. In the beginning stage, the grating is apodized from a 95% to 82% fill factor in the first four teeth, which reduces the grating's initial emission strength [10, 23]. By dampening the first stage's emission, the grating's field profile more closely matches the Gaussian mode of the vertically oriented fiber. In the second stage, the fill factor and period remain uniform for eight periods at 81% and 795 nm, respectively, and this stage is responsible for 70% of the grating's power coupling into the fiber. In the third stage, the period is chirped over six periods from 770 nm to 700 nm, and the fill factor becomes 86%. The chirp causes the third stage to emit light at a slightly negative angle of three degrees, which allows for an extra grating period to emit light into the fiber. Without this negative angle, the third stage's emission would not fit into the fiber's 10.4 µm mode field diameter. Although a three degree emission will guide into the acceptance cone of a vertically oriented fiber, this creates a focal plane above the grating and slightly reduces the vertical translation tolerance of the coupled fiber, which will be discussed later. The grating's final stage consists of a quasi-periodic DBR that reflects only 50% of light back into previous grating stages. When this stage is replaced by a uniform DBR with 99% reflectivity, the grating's overall coupling efficiency drops from 68% to 62%. This counter-intuitive result occurs because the beginning of the quasi-periodic DBR does not strongly reflect and instead emits a unique phase-front with side-lobes. When this emission is interfered with the emission from stage three, the resulting phase-front is flatter, narrower, and more Gaussian-like due to destructive interference, all of which increase the fiber coupling efficiency.

3.2 Cover-Slot Grating

Simulations for the cover-slot platform were also carried out as described in the above section. Because introducing an initial design into the genetic algorithm is detrimental, only purely random designs were fed into the simulation/optimization loop. As with the multiple-slot procedure, the simulations were initially performed with 1550 nm wavelength light. However, several of the grating designs produced by the genetic algorithm had 1.5 times the efficiency at L-band wavelengths due to longer wavelengths having less destructive interference from substrate reflections at the suboptimal 3 µm oxide thickness. In order to obtain optimal grating performance, the genetic algorithm was re-tooled to optimize for a range of wavelengths. Following this nontrivial upgrade, the genetic algorithm evaluated each grating design across the entire C-band without sacrificing simulation speed/time. Because a grating's fitness was now weighted across a wavelength range, having a flatter spectral response resulted in a design having a higher "fitness" than before.

Unlike the multi-slot design, all attempts of the cover-slot design iteration converged within 100 generations on a single design with 22% coupling efficiency, regardless of the genetic algorithm's starting point within the design space. To adequately explore the local design space around this optimum, the genetic algorithm's mutation rate was lowered to only alter a single grating tooth by +/- 10% per iteration. While this dramatically decreased the coupling efficiency improvement obtained per generation, every subsequent generation yielded a steady, monotonic increase in efficiency, indicating that a gradient descent was occurring on a smooth, well-behaved portion of the design space. After approximately 5,000 generations, the coupling efficiency improvement had plateaued at 47%. In addition, even though the genetic algorithm only evaluated designs within the C-band, the final result obtained a simulated 3 dB bandwidth of 150 nm. This overshoot of desired bandwidth is likely due to an overly stringent spectral flatness restriction in the genetic algorithm which will be relaxed in future designs. The final design is shown in Fig. 5.

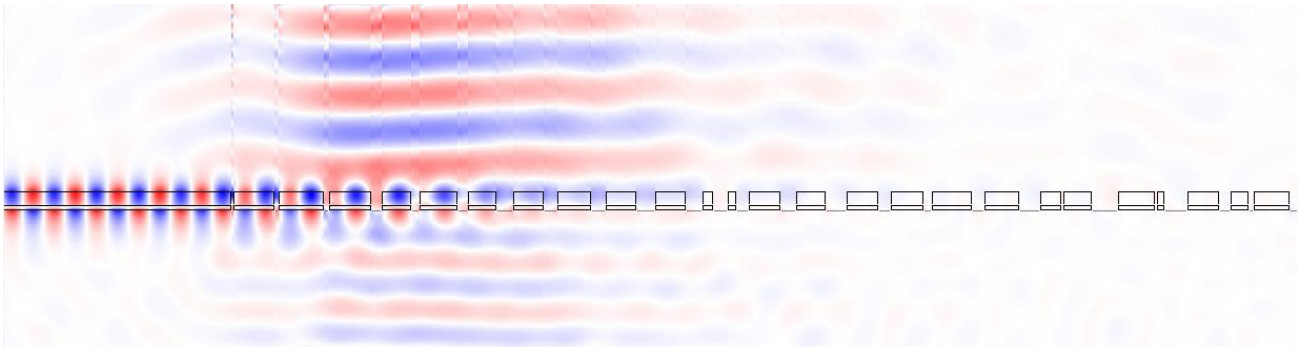

Fig. 5. Cover-slot waveguide-to-grating cross section showing simulated surface normal E-field emission to a fiber aperture from a waveguide on the left. The thin crystalline silicon waveguide is depicted with thin white rectangles, and the thicker cover-cladding of silicon nanocrystalline oxide is depicted with the larger, transparent rectangles. The etch depth for all sections is 420 nm.

4. FABRICATION

Fabrication of the multi-slot waveguide platform was previously reported in depth [27]. A top-down SEM of the completed grating is shown in Fig. 6. The cover-slot waveguide platform process began with SOI wafers provided by SOITEC which contained 250 nm thick crystalline silicon, followed by 3 µm of oxide, followed by a 500 µm thick silicon substrate. Wet thermal oxidation was performed at 1050°C followed by an HF etch to thin the top silicon layer thickness to 120 nm. Next, a 300 nm thick silicon-rich oxide layer was deposited by 34 hours of LPCVD of N_2O and silane gases at 600°C, 250 mtorr, 35 sccm of silane, and 180 sccm of N_2O. Unlike the multi-slot process, the wafer was then immediately annealed at 1150°C for three minutes, which creates smaller (~1 nm) nanocrystals with a theoretically higher Kerr effect [28]. In order to fit the samples into subsequent processing steps, the wafers were cleaved into 2x2 cm chips using a diamond-tipped scribe and glass pliers. The chip layout was then patterned in ZEP-520A resist by a 50 kV JEOL 6000 electron beam system at 100 pA. The developed resist pattern was then etched with alternating reactive-ion-etching of $CHF_3 + O_2$ and $HBr + Cl_2$ chemistry, respectively. Unlike the multi-slot fabrication, post-process analysis and error-corrected fabrication was not performed for the cover-slot grating couplers.

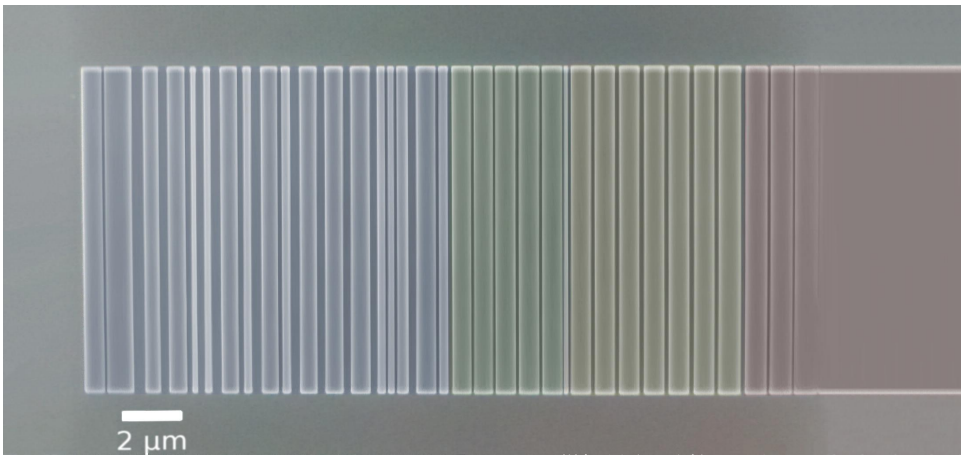

Fig. 6. Colorized SEM depicting each grating stage. Red is the apodized grating/waveguide interface, yellow is the primary fiber-coupling region, green is the secondary coupling region of chirped grating period, and blue is the quasi-periodic DBR to partially emit and reflect light back into previous grating stages.

5. RESULTS

In both chip layouts, identical 12 µm wide input/output gratings were connected to 500 µm long waveguides that adiabatically tapered their widths from 12 µm to 500 nm. These single mode waveguides were then connected via a circular 125 µm radius u-turn, as shown in Fig. 7(b). In order to characterize the gratings' spectral coupling performance, broadband TM light must be coupled and measured, as the grating coupler is designed for a horizontal slot waveguide, which requires a vertically oriented E-field (TM) to confine light into the slots. If a horizontally oriented E-field (TE) is used, the silicon layer(s) would instead guide the majority of the light. The grating would then consist of significantly different effective indices from its intended design, causing it to interfere the light from all four grating stages and emit a haphazard field profile with negligible fiber coupling efficiency. Thus, amplified spontaneous emission (ASE) spanning 1530 nm to 1620 nm and centered at 1558 nm from an erbium doped fiber array was passed through a TM polarizer and connected to a fiber array. The fiber array contained standard polarization maintaining single mode fibers that were spaced 250 µm apart. Subsequently, the array was mounted to a 6-axis stage possessing 50 nm and 0.3 arcseconds of resolution. The 2x2 cm chip containing the fabricated gratings was mounted to a standard 3-axis stage, making the chip's surface parallel to the incoming fiber array facet. The experimental coupling setup and a schematic of the fiber-grating-waveguide coupling are shown in Fig. 7.

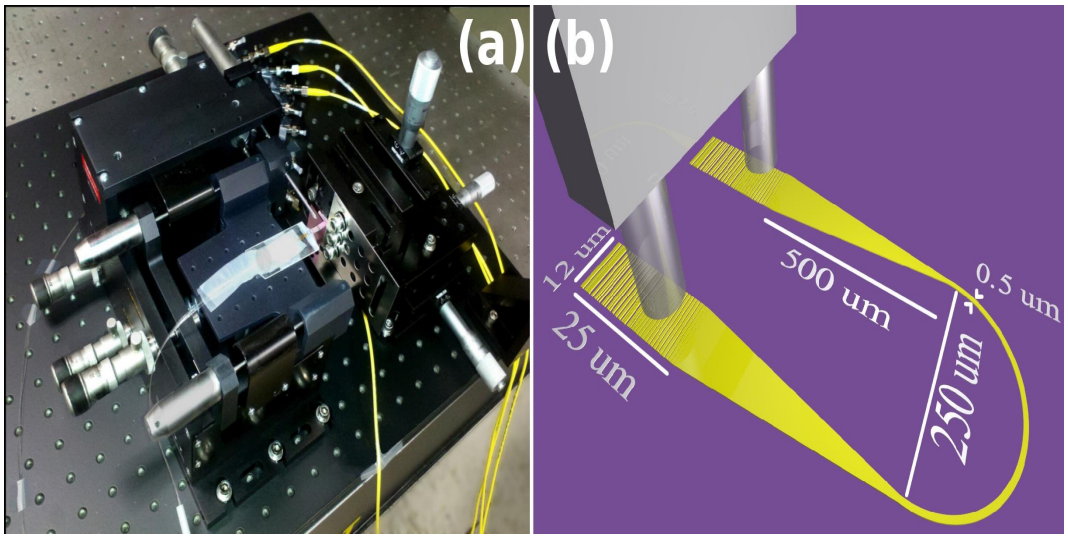

Fig. 7 (a) Experimental lab setup for perfectly normal coupling between a standard fiber array and on-chip gratings. (b) Illustrated chip layout coupled to a normally-incident input/output fiber array.

The fibers within the array were aligned approximately 2 μm above the grating couplers at perfectly normal incidence. The broadband signal was then passed through the input fiber, and an optical spectrum analyzer collected the output. The output power results were normalized to the ASE source. Ring resonators 250 nm adjacent to single mode waveguides were measured to obtain each platform's propagation loss. Any remaining loss was then allocated evenly between the input/output gratings.

For both platforms, the output power was maximized when the fiber array was exactly normal to the chip surface. The 3 dB in-plane coupling tolerance of the fiber array was approximately 2 μm in both dimensions. The measured vertical coupling tolerance was lower than the Rayleigh range of the combined grating couplers, as the total coupled power was halved when the fiber array was approximately 30 μm above the gratings. This result is likely due to the focusing effect introduced by the chirped grating stage as well as a non-Gaussian-like field arising from interfering all four grating stages at ever higher planes above the chip surfaces. It is remarkable to note that despite significant differences between the two chip platforms, both gratings ended with very similar optical alignment characteristics. Thus, the genetic algorithm's creation of 4 distinct functional grating stages in both designs, as shown in Fig. 6, is consistently apparent.

5.1 Multiple Slot Grating Results

The total loss for the entire multiple-slot grating setup was 43.4 dB. The ring resonator measurement resulted in a propagation loss of 280 dB/cm for the dual-slot single mode waveguide [27]. This extreme loss is a direct result of very high surface roughness (~20 nm) of the oxide slots, as the oxide films did not reflow during annealing due to constraining film stress with the polysilicon layers. The result is shown in Fig. 8, where a single grating of the input/output pair yielded a peak efficiency of 60.1% or -2.2 dB at 1555.8 nm. The shift from the designed 1550 nm peak is due to the final design uniformly overcompensating for the aforementioned lithography errors, leading to tooth width variance slightly exceeding trench variance during e-beam writing. The fiber array contains up to 0.5 μm of translational misalignment between its fibers, which accounts for the discrepancy between measured peak efficiency and theoretical expectation.

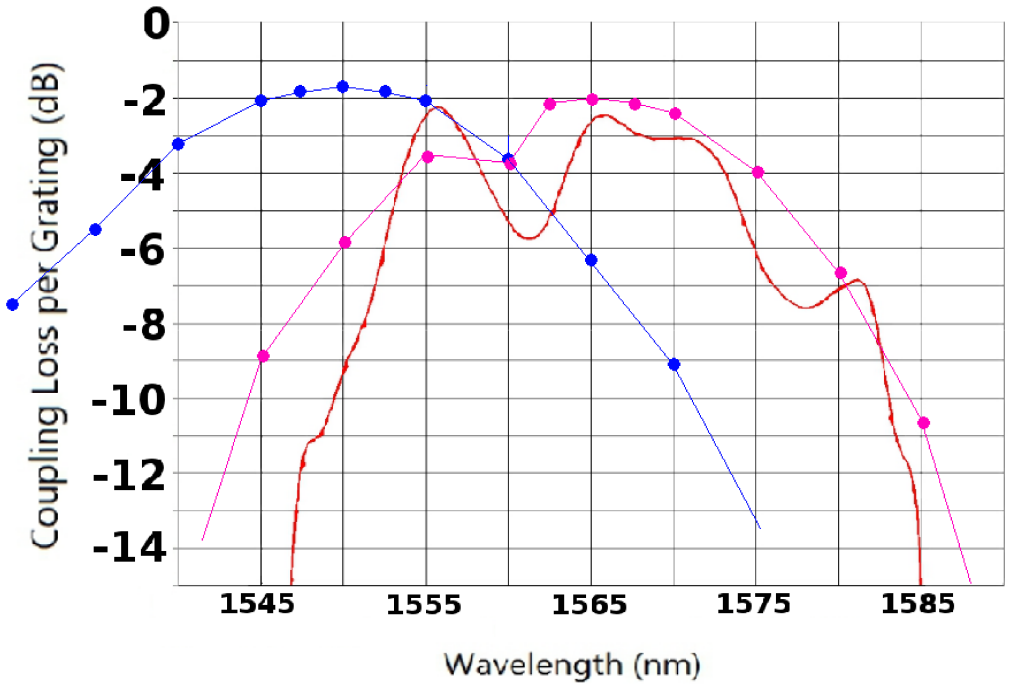

Fig. 8. Experimentally measured spectrum of single mode fiber coupling efficiency to/from a fabricated multiple horizontal slot grating. The data are normalized to the ASE source and for a single grating coupler. The experimental measurement data are in red, simulated results of the ideal grating design are in blue, and simulated results of the grating with fabrication error are in pink.

5.2 Cover Slot Grating Results

The total loss for the entire cover-slot grating setup was 24.9 dB. The ring resonator measurement resulted in a propagation loss of 120 dB/cm for the cover-slot single mode waveguide. The cover-slot's higher temperature anneal step resulted in a significant propagation loss reduction when compared to the multiple-slot waveguide propagation loss. However, the remaining propagation loss remains quite severe and is likely due to very small grain boundary formation within the oxide that is seeded by the silicon nanocrystals themselves, which act as efficient scattering centers. Because surface roughness was obviated due to the use of an atomically flat crystalline silicon interface, LPCVD of silicon nanocrystalline oxide is likely to remain a high loss platform, relegating future work to PECVD based nanocrystals that do not suffer from grain-boundary formation [5].

After normalizing for propagation loss, the cover-slot grating measurement result is shown in Fig. 9, where a single grating of the input/output pair yielded a peak efficiency of 38.7% or -4.1 dB at 1608 nm. While the simulated 1 dB bandwidth is 70 nm and 3 dB bandwidth is 150 nm, the actual spectral peak is shifted to the edge of the ASE's emission band. Presuming the actual grating coupling profile is spectrally symmetric, then the actual 1 dB bandwidth is extrapolated to be 66 nm. The dramatic spectral shift from the designed 1550 nm peak is due to several factors. First, the over-exposure of grating teeth lines leads to wider grating trenches, thereby lowering the effective index and shifting the peak to longer wavelengths. Second, the design contained overly fine lithographic features down to 30 nm, which further exacerbates the grating's trench width sensitivity. In future work, the genetic algorithm shall be further upgraded to include lithography errors in its design process. Third, the nanocrystalline oxide index was approximately 3% below its design target, which also lowers the effective index and further shifts the peak efficiency to longer wavelengths. The above issues also contribute to lowering the grating's actual peak efficiency by reducing the effectiveness of the grating's apodization and back-reflector regions. The fiber array contains up to 0.5 μm of translational misalignment between its

fibers, which also accounts for the discrepancy between measured peak efficiency and theoretical expectation.

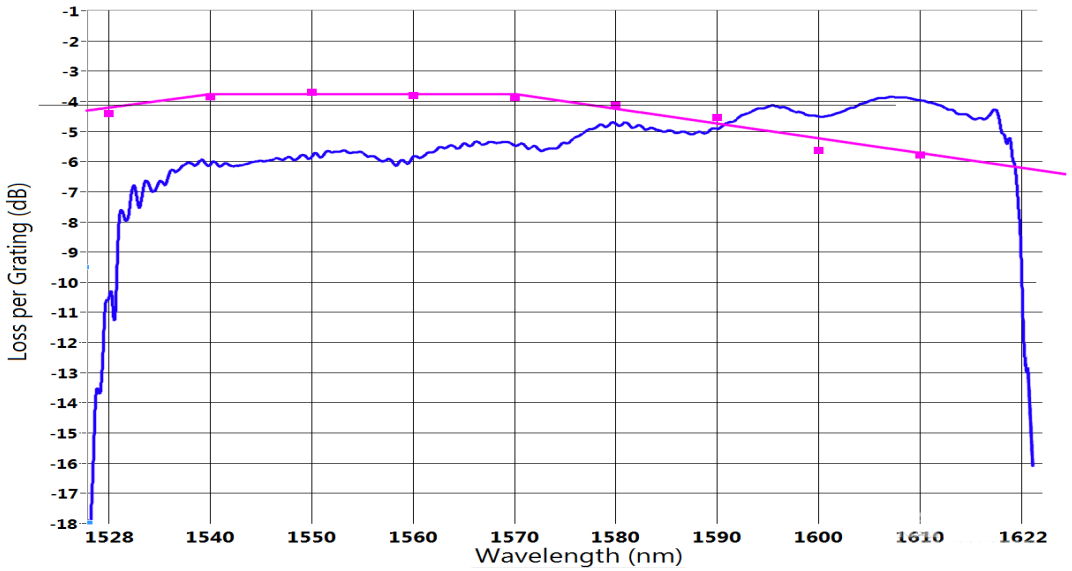

Fig. 9. Experimentally measured spectrum of single mode fiber coupling efficiency to/from a fabricated horizontal cover-slot grating. The data are normalized to the ASE source and for a single grating coupler. The experimental measurement data are in blue, and simulated results of the ideal grating design are in pink. The simulated 3 dB bandwidth is 150 nm, and the experimental measurement is source-limited to the range of 1530-1620 nm. The Fabry-Perot ripples are due to reflections from the fiber facet.

6. CONCLUSION

Efficient and broadband grating coupling from a normally incident fiber array to both multiple horizontal slot waveguides and horizontal cover-slot waveguides have been experimentally demonstrated. The multiple horizontal slot grating achieved a 60.1% experimental coupling efficiency per grating, while the cover-slot grating achieved a 38.7% experimental coupling efficiency and a 1 dB bandwidth that is likely in excess of 65 nm. Starting from purely random designs, simulations from a custom genetic algorithm created a four stage grating coupler for each waveguide platform with theoretical efficiencies of 68% and 47%, respectively. In contrast, a traditional coupler designed solely from first principles yielded a 27% theoretical efficiency and plateaued at 40% when augmented with the genetic algorithm. By then introducing wavelength variation into the genetic algorithm, a grating design with a 3 dB bandwidth of 150 nm was obtained. In the future, additional schemes incorporated into a genetic algorithm may effectively and simultaneously design around many additional constraints and/or transients imposed in the real world, including lithographic feature size and repeatability constraints. This report demonstrates the promise of genetic algorithm-based design by reducing to practice the first large bandwidth vertical grating coupler to a novel silicon nanocrystal horizontal cover-slot waveguide.

7. ACKNOWLEDGEMENTS

Financial support from the Cullen Trust For Higher Education is gratefully acknowledged. The IPKISS software suite was heavily utilized for chip layout design and is highly appreciated.

8. REFERENCES

[1] R. Guider, N. Daldosso, A. Pilanti, E. Jordana, JM. Fedeli, and L. Pavesi, “NanoSi low loss horizontal slot waveguides coupled to high Q ring resonators,” Opt. Exp. 17, 20762-20770 (2009).

[2] K. Preston, M. Lipson, "Slot waveguides with polycrystalline silicon for electrical injection," Opt. Exp. 17, No. 3, 1527 (2009).
[3] T. Baehr-Jones, M. Hochberg, C. Walker, and A. Scherer, "High-Q optical resonators in silicon-on-insulator-based slot waveguides," Appl. Phys. Lett. 86, 081101 (2005).
[4] R. Sun, P. Dong, N. Feng, .C. Hong, J. Michel, M. Lipson, L. Kimerling, "Horizontal single and multiple slot waveguides:optical transmission at λ = 1550 nm," Opt. Exp. 15, No. 26, 17967 (2007).
[5] A. Martınez, J. Blasco, P. Sanchis, J. V. Galan, J. Garcıa-Ruperez, E. Jordana, P. Gautier, Y. Lebour, S. Hernandez, R. Spano, R. Guider, N. Daldosso, B. Garrido, J. M. Fedeli, P. Lorenzo, "Ultrafast All-Optical Switching in a Silicon-Nanocrystal-Based Silicon Slot Waveguide at Telecom Wavelengths," Nano Lett. 10, 1506–1511 (2010).
[6] R. Spano, N. Daldosso, M. Cazzanelli, L. Ferraioli, L. Tartara, J.Yu, V. Degiorgio, E. Jordana, J. M. Fedeli, and L. Pavesi, "Bound electronic and free carrier nonlinearities in Silicon nanocrystals at 1550nm," Opt. Exp. 17, Issue 5, pp. 3941-3950 (2009).
[7] C. Koos, P. Vorreau, T. Vallaitis, P. Dumon, W. Bogaerts, R. Baets, B. Esembeson, I. Biaggio, T. Michinobu, F. Diederich, W. Freude, and J. Leuthold, "All-optical high-speed signal processing with silicon–organic hybrid slot waveguides," Nature Photonics 3, 216 - 219 (2009).
[8] J. Shainline and J. Xu, "Silicon as an emissive optical medium," Laser Photon. Rev. 1, No. 4, 334–348 (2007).
[9] J.V. Galan, P. Sanchis, J. Blasco, A. Martinez, J. Martí, "High efficiency fiber coupling to silicon sandwiched slot waveguides," Opt. Comm. 281, Issue 20, 5173–5175 (2008).
[10] G. Roelkens, D. Vermeulen, S. Selvaraja, R. Halir, W. Bogaerts, and D. Van Thourhout, "Grating-Based Optical Fiber Interfaces for Silicon-on-Insulator Photonic Integrated Circuits," IEEE J Sel. Top. Quant., 17, No. 3, 571 (2011).
[11] D. Taillaert, P. Bienstman, and R. Baets, "Compact efficient broadband grating coupler for silicon-on-insulator waveguides," Opt. Lett. 29, No. 23 (2004).
[12] M. Anetlius, K. B. Gylfason, and H. Sohlstr, "An apodized SOI waveguide-to-fiber surface grating coupler for single lithography silicon photonics," Opt. Exp. 19, No. 4, 3592, (2011).
[13] D. Aillaerta, F. Van Laere, M. Yre, W. Bogaerts, D. Van Thourhout, P. Bienstman, and R. Baets, "Grating Couplers for Coupling between Optical Fibers and Nanophotonic Waveguides," Jap. J Appl. Phys. 45, No. 8A, pp. 6071–6077 (2006).
[14] G.Roelkens, D.Vermeulen, D.VanThourhout, R.Baets, S.Brision, P.Lyan, P.Gautier, and J.-M.Fédéli, " High Efficiency Diffractive Grating Couplers for Interfacing a Single Mode Optical Fiber with a Nanophotonic Silicon-on-Insulator Waveguide Circuit," Appl. Phys. Lett. 92,131101 (2008).
[15] C. Xiong, W. H.P. Pernice, M. Li, and H. X. Tang, "High performance nanophotonic circuits based on partially buried horizontal slot waveguides," Opt. Exp., 18, Issue 20, pp. 20690-20698 (2010).
[16] J.V. Galan, P. Sanchis, J. Blasco, J. Marti, "Study of High Efficiency Grating Couplers for Silicon-Based Horizontal Slot Waveguides," IEEE Photonic Tech. L 20, Issue 12 985 - 987 (2008).
[17] B. Wang, J. Jiang, and G. Nordin, "Compact slanted grating couplers," Opt. Exp. 12(15) pp 3313 (2004).
[18] D. Taillaert, W. Bogaerts, P. Bienstman, T. F. Krauss, P. Van Daele, I. Moerman, S. Verstuyft, K. De Mesel, and R. Baets, "An Out-of-Plane Grating Coupler for Efficient Butt-Coupling Between Compact Planar Waveguides and Single-Mode Fibers," IEEE J. Quantum Electron. 38(7), 949 (2002).
[19] G. Roelkens, D. Van Thourhout, R. Baets, "High efficiency grating couplers between silicon-on-insulator waveguides and perfectly vertical optical fibers," Opt. Lett. 32(11), 1495-1497 (2007).
[20] H. Yamada, M. Nozawa, M. Kinoshita and K. Ohashi,"Vertical-coupling optical interface for on-chip optical interconnection," Opt. Exp. 19, No. 2, 698 (2011).
[21] G. Roelkens, D. Van Thourhout, R. Baets, "High efficiency Silicon-on-Insulator grating coupler based on a poly-Silicon overlay," Opt. Exp. 14(24) 11622-11630 (2006).
[22] D. Goldberg, *Genetic Algorithms in Search, Optimization, and Machine Learning* (Addison-Wesley, 1989).
[23] Y. Tang, Z. Wang, L. Wosinski, U. Westergren, S. He, "Highly Efficient Nonuniform Grating Coupler for Silicon-on-Insulator Nanophotonic Circuits," Opt. Lett. 35, No. 8, 1290 (2010).
[24] D. Kwong, J. Covey, A. Hosseini, Y. Zhang, X. Xu, R.T. Chen, "Ultralow-loss polycrystalline silicon waveguides and high uniformity 1x12 MMI fanout for 3D photonic integration," Opt. Exp. 20(19) 21722 (2012).

[25] P. Bienstman, R. Baets, "Optical modelling of photonic crystals and VCSELs using eigenmode expansion and perfectly matched layers," Opt. Quant. Elec. 33, 327-341 (2001).
[26] J. Ctyroky, S. Helfert, R. Pregla, P. Bienstman, R. Baets, R. De Ridder, R. Stoffer, G. Klaasse, J. Petracek, P. Lalanne, J.-P. Hugonin, R.M. De La Rue, "Bragg waveguide grating as a 1D photonic band gap structure: COST 268 modelling task," Opt. Quant. Elec. 34, (5/6), p.455-470 (2002).
[27] J. Covey, R.T. Chen, "Efficient perfectly vertical fiber-to-chip grating coupler for silicon horizontal multiple slot waveguides," Opt. Exp. 21(9) 10886 (2013).
[28] K. Koukos, E. B. Edel-Pereira, O. G. Authier-Lafaye, E. Scheid, L. Bouscayrol, B. F. Ranc, P. Arguel, S. Bonnefont, F. Lozes-Dupuy, and G. Sarrabayrous, "Effect of Annealing Conditions on Photoluminescence Properties of Low-Pressure Chemical Vapour Deposition-Grown Silicon Nanocrystals," Jap. J Appl. Phys. 47, No. 1, 130-132 (2008).